



# Inhibition of histone deacetylase 5 ameliorates abnormalities in 16p11.2 duplication mouse model

Benjamin Rein, Megan Conrow-Graham, Allea Frazier, Qing Cao, Zhen Yan\*

Department of Physiology and Biophysics, State University of New York at Buffalo, Jacobs School of Medicine and Biomedical Sciences, Buffalo, NY, 14214, USA

## ARTICLE INFO

### Keywords:

16p11.2 duplication  
Autism spectrum disorder  
HDAC5  
GABA  
Prefrontal cortex  
LMK235  
Npas4

## ABSTRACT

Microduplication of the human 16p11.2 gene locus is associated with a range of neurodevelopmental outcomes, including autism spectrum disorder (ASD). Mice carrying heterozygous 16p11.2 duplication (16p11.2<sup>dp/+</sup>) display social deficits, which is attributable to impaired GABAergic synaptic function in prefrontal cortex (PFC) driven by downregulation of *Npas4*, an activity-dependent transcription factor that regulates GABA synapse formation. However, the molecular mechanisms underlying the diminished transcription of *Npas4* in 16p11.2 duplication remain unknown. *Npas4* is one of the target genes regulated by histone deacetylase 5 (HDAC5), an epigenetic enzyme repressing gene expression via removal of transcription-permissive acetyl groups from histones. Here we report that HDAC5 expression is elevated and histone acetylation is reduced at the *Npas4* promoter in PFC of 16p11.2<sup>dp/+</sup> mice. Treatment with the HDAC5 inhibitor LMK235 normalizes histone acetylation, restores GABAergic signaling in PFC, and significantly improves social preference in 16p11.2<sup>dp/+</sup> mice. These findings suggest that HDAC5 inhibition is a promising therapeutic avenue to alleviate genetic, synaptic and behavioral deficits in 16p11.2 duplication conditions.

## 1. Introduction

Duplication of the human 16p11.2 genetic locus (chromosome 16, position 11.2) is associated with a range of neurodevelopmental disorders, including autism spectrum disorder (ASD) (Rein and Yan, 2020). The neurobiology of 16p11.2 duplications is complex and unclear, as it involves the genetic duplication of ~27 genes with many respective downstream effectors. Thus, identifying unifying, core pathologies which may be amenable to pharmacological therapy is of great translational importance.

Our previous studies have found that mice with heterozygous duplication of the genetic region syntenic to human 16p11.2 (16p11.2<sup>dp/+</sup> mice) display social and cognitive impairments, along with GABAergic synaptic deficits in the prefrontal cortex (PFC) (Rein et al., 2021), a brain region critically involved in ASD pathology (Yan and Rein, 2021). *Npas4*, an activity-dependent transcription factor that promotes GABA synapse formation (Bloodgood et al., 2013; Lin et al., 2008) and displays high expression in frontal cortex (Damborsky et al., 2015), is downregulated in mPFC of 16p11.2<sup>dp/+</sup> mice. Restoring *Npas4* expression is sufficient to ameliorate both the synaptic and behavioral deficits in 16p11.2<sup>dp/+</sup> mice (Rein et al., 2021). Thus, we speculate that

elevation of *Npas4* may offer therapeutic potential for the social and cognitive deficits associated with 16p11.2 duplications. However, direct pharmacological manipulation of *Npas4* may be unattainable, as its expression is primarily neuronal activity-dependent (Bloodgood et al., 2013; Lin et al., 2008). As such, the identification of upstream regulators of *Npas4* transcription may have translational value for the treatment of 16p11.2 duplication and other related disorders.

Transcriptional regulation of gene expression is partially mediated by epigenetic enzymes that enact post-translational modifications on DNA-packaging proteins called histones (Jenuwein and Allis, 2001). These modifications, such as histone acetylation or methylation, alter DNA accessibility and thereby induce transcriptional activation or repression. Inhibition of class I histone deacetylases (HDACs) has been shown to ameliorate social deficits in mice with deficiency of the autism-risk gene *Shank3* (Ma et al., 2018; Qin et al., 2018). Additionally, a screening of nearly 1500 compounds in human iPSC-derived cortical neurons from patients with the autism-linked 7q11.23 duplication revealed that three HDAC inhibitors normalized the expression of a critical gene transcript driving 7q11.23 pathogenesis, suggesting that they may offer therapeutic potential (Cavallo et al., 2020). Interestingly, the class II histone-deacetylase 5 (HDAC5), has been shown to regulate

\* Corresponding author.

E-mail address: [zhenyan@buffalo.edu](mailto:zhenyan@buffalo.edu) (Z. Yan).

*Npas4* expression by directly suppressing its activity-dependent induction in the nucleus accumbens (Taniguchi et al., 2017). We thus sought to explore whether HDAC5 dysregulation may be responsible for *Npas4* downregulation and the associated GABA deficits in PFC of 16p11.2<sup>dp/+</sup> mice.

In the current study, we investigated the relationship between HDAC5 and *Npas4* in 16p11.2<sup>dp/+</sup> and evaluated the therapeutic efficacy of HDAC5 inhibition. We report that abnormal HDAC5 overexpression in 16p11.2<sup>dp/+</sup> PFC appears to promote *Npas4* downregulation via reducing the acetylation at *Npas4* promoter. Furthermore, systemic administration of the HDAC5 inhibitor LMK235 is sufficient to elevate PFC GABAergic synaptic transmission and enhance sociability in 16p11.2<sup>dp/+</sup> mice. Therefore, pharmacological inhibition of HDAC5 may offer therapeutic potential for the treatment of 16p11.2 duplication and perhaps other related disorders.

## 2. Materials and methods

### 2.1. Animals and drugs

16p11.2<sup>dp/+</sup> mice carrying a heterozygous duplication of the 7F3 chromosomal region homologous to human 16p11.2 were generated as previously described (Horev et al., 2011). 16p11.2<sup>dp/+</sup> mice were initially generated on a hybrid C57BL/6 N:129Sv background before being backcrossed more than 10 generations onto the C57BL/6 inbred strain and subsequently maintained on the C57BL/6 genetic background. Thus, the WT and 16p11.2<sup>dp/+</sup> animals used in the current study represent a pure C57BL/6 background. All animals were group-housed with 1–3 sex-matched conspecifics of either genotype (WT or 16p11.2<sup>dp/+</sup>) and provided standard enrichment. Animals were maintained on a 12-h light (6:00 a.m.–6:00 p.m.)/dark (6:00 p.m.–6:00 a.m.) cycle. In all experiments, 7–9-week-old (both male and female) 16p11.2<sup>dp/+</sup> mice and wild-type (WT) littermates were used. Similar results were obtained from 16p11.2<sup>dp/+</sup> mice of either sex, so results were pooled together. Animal studies were performed with the approval of the Institutional Animal Care and Use Committee (IACUC) of the State University of New York at Buffalo.

LMK235 (Tocris) was dissolved into DMSO (28.57 mg/ml), then diluted with 0.9% saline to 0.5 mg/ml before injection. LMK235 (5 mg/kg) was administered via intraperitoneal injection three times, once daily over three subsequent days. Injections were spaced approximately 24 h apart. Previous studies indicate that LMK235 crosses the blood-brain-barrier and elevates hippocampal histone acetylation at doses of both 5 mg/kg and 20 mg/kg (Trazzi et al., 2016), and exerts similar behavioral effects on ethanol consumption at either dose (Pozhidayeva et al., 2020). Thus, a dosage of 5 mg/kg was chosen for the current study. Behavioral, biochemical, and electrophysiological studies were performed between 1 and 5 days following the final injection.

### 2.2. Quantitative real-time RT-PCR

Total RNA was isolated from mouse PFC punches using Trizol reagent (Invitrogen) and treated with DNase I (Invitrogen) to remove genomic DNA. SuperScript III first-strand synthesis system for RT-PCR (Invitrogen) was used to reverse-transcribe mRNA into cDNA, followed by treatment with RNase H (2 U/I) for 20 min at 37 °C. Quantitative real-time RT-PCR was performed using the iCycler iQ™ Real-Time PCR Detection System and iQ™ Supermix (Bio-Rad) according to the manufacturer's instructions. GAPDH was used as the housekeeping gene for quantitation of the expression of target genes in samples from WT vs. 16p11.2<sup>dp/+</sup> mice. Fold changes in the target genes were determined by:  $\text{Fold change} = 2^{-\Delta(\Delta\text{CT})}$ , where  $\Delta\text{CT} = \text{CT}(\text{target}) - \text{CT}(\text{GAPDH})$ , and  $\Delta(\Delta\text{CT}) = \Delta\text{CT}(\text{treated group}) - \Delta\text{CT}(\text{WT})$ . CT (threshold cycle) is defined as the fractional cycle number at which the fluorescence reaches 10× the standard deviation of the baseline. A total reaction mixture of 20 μL was amplified in a 96-well thin-wall PCR plate (Bio-Rad) using the

following PCR cycling parameters: 95 °C for 5 min followed by 40 cycles of 95 °C for 30 s, 55 °C for 30 s, and 72 °C for 60 s. Primers for target genes are as follows:

Gene	Forward	Reverse
<i>Gapdh</i>	GACAACCTCACTCAAGATTGTCTAG	ATGGCATGGACTGTGGTCATGAG
<i>Hdac2</i>	CTGCCTATCCCGCTCTGTG	TGCCAATATCACCATCATAGTAGT
<i>Hdac3</i>	GCATTCCGAGGACATGGGGAA	GGAGTGTGAAATCTGGGGCA
<i>Hdac4</i>	CCTGCCGCTGGTGCG	GACAAGGGGTGTCTGGGTG
<i>Hdac5</i>	GTGTCCAGTCCGTTGTTTGC	GTGGACCAAAGTCTGGGTGG
<i>Hdac9</i>	GGAGCTAGACGCCAGTTTA	GCCACTCCATCTGTGTGCAA

### 2.3. Immunohistochemistry

Mice were anesthetized and transcardially perfused with PBS followed by 4% paraformaldehyde (PFA) before brain removal. Brains were post-fixed in 4% PFA for 2 days and cut into 30 μm slices. Slices were cut coronally and washed and blocked for 1 h in PBS containing 5% donkey serum and 0.3% Triton for permeabilization. After washing, slices were incubated with the primary antibody against HDAC5 (1:500, Abcam, Ab1439) or acetylated histone 3 (1:1000, Cell Signaling Technology, 9441) for 48 h at 4 °C. After washing three times (30 min with gentle shaking) in PBS, slices were incubated with secondary antibody (Alexa Fluor 568, Invitrogen, ab175470 [donkey-anti-rabbit], 1:1000) for 1 h at room temperature, followed by three washes with PBS. Slices were mounted on slides with Vectashield mounting media with DAPI (Vector Laboratories). Images were acquired using a Leica DMi8 fluorescence microscope. All specimens were imaged under identical conditions and analyzed with identical parameters using ImageJ software.

### 2.4. Western blotting of nuclear proteins

Nuclear extracts from mouse brains were prepared as previously described (Rein et al., 2021). Eight prefrontal cortex punches (diameter: 2 mm) from fresh mouse brain slices (300 μm) per animal were collected and homogenized with 500 μL homogenization buffer (20 mM Tris-HCl, pH 7.4, 10 mM NaCl, 3 mM MgCl<sub>2</sub>, 0.5% NP-40, 1 mM PMSF, with cocktail protease inhibitor). The homogenate was incubated on ice for 15 min and followed by centrifugation at 3000 g, 4 °C for 10 min. The nuclear pellet was resuspended in 50 μL nuclear extract buffer (100 mM Tris-HCl, pH 7.4, 100 mM NaCl, 1 mM EDTA, 1% Triton X-100, 0.1% SDS, 10% glycerol, 1 mM PMSF, with cocktail protease inhibitor) and incubated on ice for 30 min with periodic vortexing to resuspend the pellet. After centrifugation, the supernatant for nuclear fractions was collected, boiled in 2 × SDS loading buffer for 5 min and then separated on 10% SDS-polyacrylamide gels. Western blotting experiments for nuclear proteins were performed with antibodies against total histone 3 (1:1000, Cell Signaling Technology, 4499), and acetylated histone 3 (1:1000, Cell Signaling Technology, 9441).

### 2.5. Chromatin immunoprecipitation

For the ChIP-PCR assay of histone acetylation at *Npas4* gene promoter, chromatin was extracted by first thoroughly homogenizing eight PFC punches from each mouse in 250 μL douncing buffer (10 mM Tris-HCl, 4 mM MgCl<sub>2</sub>, 1 mM CaCl<sub>2</sub>) by passing 10 times through a 26-gauge syringe. The sample was then incubated with 12.5 μL of micrococcal nuclease (MNase, 5U/ml), then placed into a 37 °C incubator for 7 min 5 μL of 0.5 M EDTA was then added. The sample was then diluted into 1 ml hypotonic buffer (0.2 mM EDTA, 0.1 mM benzaminide, 0.1 mM PMSF, 1.5 mM DTT, protease inhibitor) and incubated on ice for 60 min, with brief vortexing at 10-min intervals. The sample was then centrifuged at 3000 g for 5 min at 4 °C, and the supernatant was saved. Next, 125 μL of 10× incubation buffer was added (50 mM EDTA, 200 mM Tris Cl, 500 mM NaCl), and 137.5 μL (10% of the sample volume) was removed (input control). The remaining sample was then pre-cleared as

follows: the sample was incubated with 80  $\mu$ l of Protein A Agarose/Salmon Sperm treated Sepharose Beads (16–157 Millipore) for 2 h at 4 °C. After centrifugation at 700g for 2 min, the supernatant was transferred to a new tube. The supernatant was then incubated overnight at 4 °C with pan-acetylated H3 antibody (Cell Signaling Technology, 9441). The following morning, 40  $\mu$ l of Sepharose Beads was added, and the sample was rotated for 2 h at 4 °C. After a brief centrifugation (700 g, 2 min), the supernatant was discarded. The beads were then washed with 1 ml low salt washing buffer, then 1 ml high salt washing buffer, then 1 ml LiCl buffer, and finally 1 ml TE buffer (Millipore, 17–245). The washing process was then repeated a second time. DNA was then eluted by adding 100  $\mu$ l of elution buffer (1% SDS, 0.1 M NaHCO<sub>3</sub>) and vortexing, before incubating at room temperature for 15 min with rotation. The supernatant was then separated into a fresh tube, and the beads were subjected to another 100  $\mu$ l of elution buffer, with 15 min of rotation at room temperature. The supernatant was added to the previously obtained supernatant. Next, 8  $\mu$ l 5 M NaCl, 4  $\mu$ l 0.5 M ETA, 8  $\mu$ l Tris-HCl (Millipore, 17–245) and 1  $\mu$ l 20 mg/ml Proteinase K (Invitrogen, 25,530–049) were added to each sample. 1  $\mu$ l 20 mg/ml Proteinase K was added to previously stored input controls. All samples were incubated for 1 h at 50 °C. The QIAquick PCR purification kit was then used to recover purified DNA elutes. Purified DNA was subjected to qPCR reactions with three primers against mouse *Npas4*:

**Primer 1** (–1245 bp ~ –1194 bp relative to TSS; Forward: 5'-GAAAGGTGTATGTTGTGCCT -3'; Reverse: 5'-CATCTTTAGCTC-CAGGGCTCC -3')

**Primer 2** (–1928 bp ~ –1873 bp relative to TSS; Forward: 5'-TACCCCTGCTTTTCACTCC-3'; Reverse: 5'-GTGGTCAA-GAAACCCCTGTTC-3')

**Primer 3** (–426 bp ~ –328 bp relative to TSS; Forward: 5'-AGCCCCTTCTCATCCTTTGC-3'; Reverse: 5'-AGGGTGGTCT-GAAGCCCTTA-3')

## 2.6. Electrophysiological recordings

Whole-cell voltage-clamp recording was used to measure synaptic currents in layer V medial PFC (prelimbic and infralimbic) pyramidal neurons as previously described (Tan et al., 2019; Wang et al., 2018). Mouse brain slices (300  $\mu$ m) were positioned in a perfusion chamber attached to the fixed stage upright microscope (Olympus) and submerged in continuously flowing oxygenated ACSF (in mM: 130 NaCl, 26 NaHCO<sub>3</sub>, 1 CaCl<sub>2</sub>, 5 MgCl<sub>2</sub>, 3 KCl, 1.25 NaH<sub>2</sub>PO<sub>4</sub>, 10 glucose, pH 7.4, 300 mOsm). For IPSC recordings, 25  $\mu$ M CNQX was added into the ACSF. The pipette contained the following internal solution (in mM: 100 CsCl, 30 N-methyl-D-glucamine, 10 HEPES, 4 NaCl, 1 MgCl<sub>2</sub>, 5 EGTA, 2 QX-314, 12 phosphocreatine, 5 MgATP, 0.5 Na<sub>2</sub>GTP, pH 7.2–7.3, 265–270 mOsm). Cells were held at –70 mV. Evoked synaptic currents were generated with a pulse from a stimulation isolation unit controlled by an S48 pulse generator (Grass Technologies, West Warwick, RI). A bipolar stimulating electrode (FHC, Bowdoinham, ME) was placed ~100  $\mu$ m from the neuron under recording. Input-output responses of synaptic currents were elicited by a series of pulses with varying stimulation intensities (30–110 V) delivered at 0.20 Hz.

## 2.7. Behavioral testing

All testing was performed in a dimly lit room. The testing apparatuses were wiped with 75% ethanol between animals and trials. The Anymaze tracking software (Stoelting, Wood Dale, IL) was used to track and record behaving animals and generate heat maps. All scoring was performed manually by researchers blind to both genotypes and treatments.

The 3-chamber social preference test was performed as previously described (Rein et al., 2020). Briefly, the test mouse was first placed into a Plexiglass arena (L: 101.6 cm, W: 50.8 cm, H: 50.8 cm) containing two empty inverted pencil cups for a 10-min habituation period. On the

following day, the mouse was reintroduced to the apparatus for a 10-min trial in which the pencil cups contained two identical objects. The animal was then returned to its home cage for 5 min. The animal was then placed into the apparatus for a 10-min trial (social preference test), in which one cup contained a novel object (non-social stimulus) while the other contained an age- and sex-matched WT mouse (social stimulus). The amount of time spent interacting with each stimulus was recorded. The preference index was calculated as (social time – non-social time)/(social time + non-social time). All behavioral testing was performed on at least 3 independent cohorts.

## 2.8. Statistical analyses

All statistical analyses were performed with GraphPad Prism software. Experiments with more than two groups were subjected to one-way ANOVA, two-way ANOVA, or three-way ANOVA with Bonferroni correction for multiple post-hoc comparisons. Experiments with two groups were analyzed statistically using two-tailed unpaired *t*-tests, unless the data failed Shapiro-Wilk tests for normality, in which case the data were subjected to Mann-Whitney U tests. All data are presented as the mean  $\pm$  S.E.M. Data points identified as statistically significant outliers (determined by Grubb's test,  $p < 0.05$ ) were removed from the analyses. Sample sizes were determined based on power analyses and were similar to those reported in previous works (Wang et al., 2018; Yuen et al., 2012). The variance between groups being statistically compared was similar.

## 3. Results

### 3.1. Elevated *Hdac5* and reduced histone acetylation contribute to *Npas4* downregulation in PFC of 16p11.2<sup>dp/+</sup> mice

We have previously reported that downregulation of the GABA synapse regulator *Npas4* in prefrontal cortex (PFC) of 16p11.2 duplication mice (16p11.2<sup>dp/+</sup>) results in GABAergic synaptic impairment, which is associated with social and cognitive deficits (Rein et al., 2021). Chromatin immunoprecipitation sequencing (ChIP-seq) experiments performed by Taniguchi et al. (2017) revealed that HDAC5, a class II histone deacetylase, strongly and preferentially binds to an *Npas4* enhancer site in neurons. Interestingly, 12 of the 254 identified gene-associated HDAC5 binding sites overlap with significantly downregulated genes in 16p11.2<sup>dp/+</sup> PFC from our previous RNA-sequencing data (Rein et al., 2021), including four of the top 12 genes most strongly-regulated by HDAC5 (Fig. 1A). In contrast, none of the HDAC5-regulated genes exhibited transcriptional upregulation in 16p11.2<sup>dp/+</sup> PFC (data not shown). We therefore hypothesized that transcriptional downregulation of various genes in 16p11.2<sup>dp/+</sup> PFC mice may be linked to aberrant histone deacetylation by HDAC5.

To assess the altered expression of class I/II HDACs in 16p11.2<sup>dp/+</sup>, we performed quantitative polymerase chain reaction (qPCR). *Hdac5* mRNA level was significantly elevated in PFC of 16p11.2<sup>dp/+</sup> mice, relative to WT animals (Fig. 1B;  $n = 12$ –13 mice/group,  $t_{(23)} = 2.60$ ,  $p = 0.016$ , unpaired two-tailed *t*-test), whereas mRNA levels of other class I HDACs (*Hdac2* and *Hdac3*) and class II HDACs (*Hdac4* and *Hdac9*) were unchanged (Fig. 1B;  $n = 7$ –12 mice/group; *Hdac2*:  $t_{(16)} = 1.29$ ,  $p = 0.22$ ; *Hdac3*:  $t_{(17)} = 0.98$ ,  $p = 0.34$ ; *Hdac4*:  $t_{(22)} = 0.49$ ,  $p = 0.63$ ; *Hdac9*:  $t_{(19)} = 1.26$ ,  $p = 0.22$ , unpaired two-tailed *t*-tests). Thus, there appears to be a selective upregulation of *Hdac5* in 16p11.2 PFC.

We next performed HDAC5 immunostaining in PFC of WT and 16p11.2<sup>dp/+</sup> mice. Consistent with our qPCR data, HDAC5 fluorescence intensity was significantly elevated in 16p11.2<sup>dp/+</sup> PFC neurons, relative to WT animals (Fig. 1C;  $n = 16$ –19 slices/3–4 mice per group;  $t_{(33)} = 5.42$ ,  $p < 0.0001$ , unpaired two-tailed *t*-test). To determine whether *Hdac5* upregulation functionally impacts histone acetylation, we performed western blotting for levels of pan-histone 3 acetylation (H3Ac) in nuclear fraction of PFC. Relative to WT mice, the level of H3Ac in

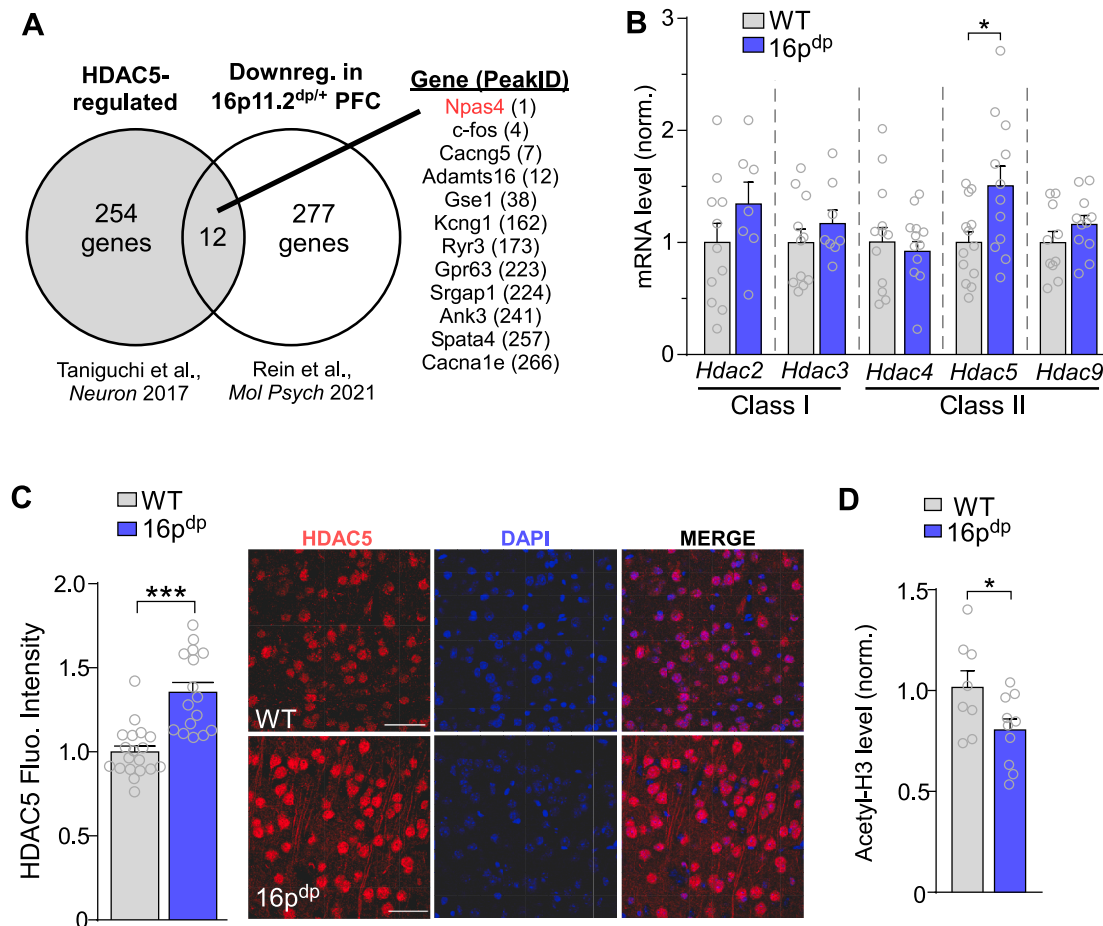


**Fig. 1.** Hdac5 is upregulated and histone acetylation is reduced in PFC of 16p11.2<sup>dp/+</sup> mice. **A**, Venn diagram showing overlap between Hdac5-associated target genes identified via ChIP-seq (Taniguchi et al., 2017) and downregulated genes in 16p11.2<sup>dp/+</sup> PFC identified via RNA-seq (Rein et al., 2021). Inset: 12 overlapping genes between the two datasets listed in order of their relative HDAC5 peak occupancy (PeakID). **B**, Bar graph comparing mRNA level of several class I and class II Hdac family members between WT and 16p11.2<sup>dp/+</sup> PFC. **C**, Bar graph comparing HDAC5 fluorescence intensity in PFC neurons between WT and 16p11.2<sup>dp/+</sup> mice. Inset: representative images showing HDAC5 (red), DAPI (blue) and merge. Scale bar: 50  $\mu$ m. **D**, Bar graph comparing acetylated histone 3 (H3Ac) level in nuclear fractions isolated from WT and 16p11.2<sup>dp/+</sup> PFC. All data are presented as mean  $\pm$  SEM. \* $p$  < 0.05, \*\*\* $p$  < 0.0001.

16p11.2<sup>dp/+</sup> PFC was significantly reduced (Fig. 1D,  $n$  = 8–10 mice/group,  $t_{(16)} = 2.22$ ,  $p = 0.041$ , unpaired two-tailed  $t$ -test), indicating that HDAC5 elevation results in reduced histone acetylation in 16p11.2<sup>dp/+</sup> PFC.

As HDAC5 is elevated in 16p11.2<sup>dp/+</sup> mice, we next examined whether pharmacological inhibition of HDAC5 could restore histone acetylation. We selected the potent HDAC5 inhibitor LMK235 (Tocris) which displays high specificity for HDAC5 (IC<sub>50</sub> = 4.22 nM). LMK235 has been shown to effectively cross the blood-brain-barrier (Trazzi et al., 2016) and has been shown to exert similar behavioral (Pozhidayeva et al., 2020) and biochemical (Trazzi et al., 2016) effects at dosages of 5 mg/kg and 20 mg/kg. We thus chose to use a dosage of 5 mg/kg (administered for three subsequent days) for the current study. To evaluate whether LMK235 was effectively crossing the blood-brain barrier and enacting functional inhibition of HDAC5, we assessed H3Ac in PFC of LMK235-treated mice via immunostaining. Consistent with western blot data, vehicle-injected 16p11.2<sup>dp/+</sup> mice displayed significantly reduced H3Ac levels in PFC, relative to vehicle-injected WT; however, 16p11.2<sup>dp/+</sup> mice treated with LMK235 displayed significantly elevated H3Ac fluorescence intensity (Fig. 2A,  $n$  = 3 mice/12–21 slices per group,  $F_{\text{interaction}(1,65)} = 8.20$ ,  $p = 0.006$ , two-way ANOVA), suggesting that systemic LMK235 restores global histone acetylation in PFC.

To validate the link between *Npas4* downregulation and histone deacetylation, we performed chromatin immunoprecipitation (ChIP)-

PCR to measure histone 3 acetylation (H3Ac) at the promoter region of *Npas4*. A significant reduction of H3Ac occupancy was observed at the *Npas4* promoter (detected by primer 1) in 16p11.2<sup>dp/+</sup> PFC (Fig. 2B,  $n$  = 10–12 mice/group;  $t_{(20)} = 2.32$ ,  $p = 0.03$ , unpaired two-tailed  $t$ -test). Next, we tested whether treatment with LMK235 was sufficient to restore *Npas4* acetylation in 16p11.2<sup>dp/+</sup> PFC. We found a trending increase in H3Ac occupancy at the *Npas4* promoter following LMK235 administration (Fig. 2C,  $n$  = 6–8 mice/group,  $t_{(12)} = 1.51$ ,  $p = 0.15$ ). These data suggest that HDAC5-mediated histone deacetylation at *Npas4* promoter may be driving *Npas4* downregulation, and HDAC5 inhibition has the potential to restore *Npas4* expression.

### 3.2. HDAC5 inhibition restores GABAergic synaptic transmission and ameliorates social deficits in 16p11.2<sup>dp/+</sup> mice

Since HDAC5 inhibition elevates *Npas4* histone acetylation in PFC of 16p11.2<sup>dp/+</sup> mice, we hypothesized that HDAC5 inhibition would relieve the transcriptional repression of *Npas4*, allowing for its typical activity-dependent expression and the resultant formation of new GABA synapses (Lin et al., 2008). To assess whether treatment with LMK235 was sufficient to restore GABAergic synaptic transmission in PFC of 16p11.2<sup>dp/+</sup> mice, we performed whole-cell patch clamp recordings in layer V PFC pyramidal neurons. Relative to WT mice, 16p11.2<sup>dp/+</sup> mice displayed significantly reduced amplitudes of GABA<sub>A</sub> receptor-mediated inhibitory postsynaptic currents (GABA<sub>A</sub>-IPSC) evoked by a series of

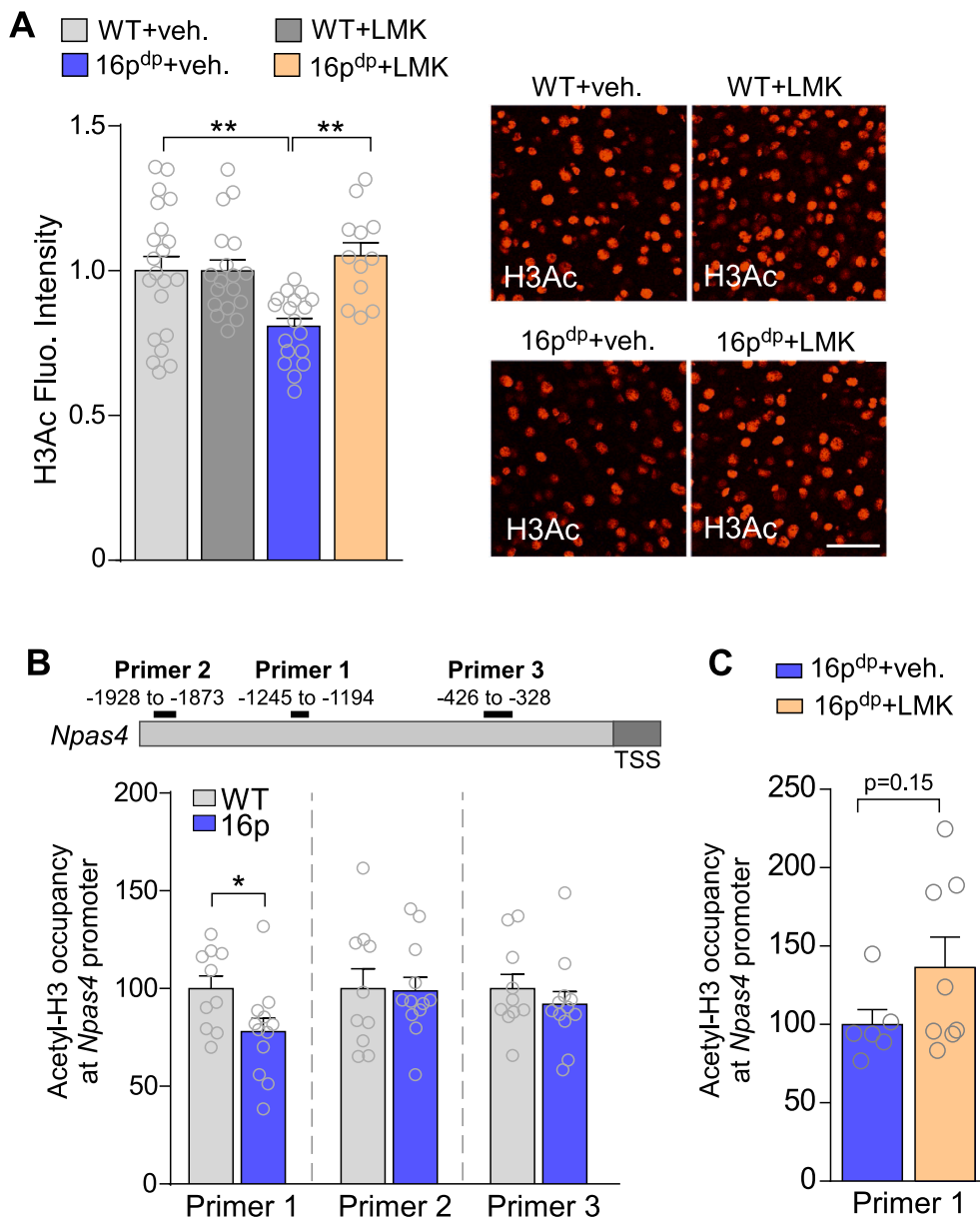


**Fig. 2.** Systemic administration of the HDAC5 inhibitor LMK235 restores histone acetylation. **A**, Bar graph comparing H3Ac fluorescence intensity in WT and 16p11.2<sup>dp/+</sup> mice treated with vehicle or LMK235. Inset: Representative images showing H3Ac immunofluorescence. Scale bar: 50  $\mu$ m. **B**, Bar graph comparing occupancy of H3Ac at three regions upstream of the TSS (Transcription Start Site) of *Npas4* between WT and 16p11.2<sup>dp/+</sup> PFC assayed via chromatin immunoprecipitation (ChIP). **C**, Bar graph comparing occupancy of H3Ac at a promoter region of *Npas4* between 16p11.2<sup>dp/+</sup> mice treated with vehicle or LMK235. All data are presented as mean  $\pm$  SEM. \* $p < 0.05$ , \*\* $p < 0.01$ .

stimulation intensities, however, GABA<sub>A</sub>R-IPSC amplitudes were significantly elevated in 16p11.2<sup>dp/+</sup> mice treated with LMK235 (Fig. 3A and B, 3–4 mice/17–20 cells per group,  $F_{\text{group}}(2,54) = 6.26, p = 0.004$ , two-way ANOVA), indicating the recovery of synaptic inhibition in PFC of 16p11.2<sup>dp/+</sup> mice by HDAC5 inhibition.

Next, we examined the rescue effect of HDAC5 inhibition on behavioral deficits in 16p11.2<sup>dp/+</sup> mice. In our previous study, we found that elevating GABAergic signaling in PFC via viral upregulation of *Npas4* reversed social deficits, while other behavioral phenotypes, such as self-grooming, were unaffected in these animals (Rein et al., 2021). Therefore, we chose to specifically evaluate the effect of LMK235 administration on social behaviors in 16p11.2<sup>dp/+</sup> mice. We selected the three-chamber social preference test, which evaluates the animal's preference for a social stimulus over a non-social stimulus (Rein et al., 2020) and appears to be highly sensitive to synaptic dysfunction in PFC (Qin et al., 2018; Wang et al., 2020, 2021). The 16p11.2<sup>dp/+</sup> mice display pronounced deficits in this task, which can be ameliorated by elevating GABAergic signaling in PFC (Rein et al., 2021). Since LMK235 elevates GABAergic signaling in 16p11.2<sup>dp/+</sup> PFC (Fig. 3), we intended to assess whether these synaptic alterations were conferring measurable

changes in relevant behavioral readouts. Vehicle-treated 16p11.2<sup>dp/+</sup> mice displayed a significantly lower social preference index relative to vehicle-treated WT, however, LMK235-treated 16p11.2<sup>dp/+</sup> mice showed significant improvement, with no difference from WT (Fig. 4A,  $n = 7$ –12 mice/group,  $F_{\text{interaction}}(1,36) = 6.448, p = 0.016$ , two-way ANOVA). The social preference index was unchanged in LMK235-treated WT mice. Correspondingly, vehicle-treated 16p11.2<sup>dp/+</sup> mice spent significantly less time than vehicle-treated WT mice interacting with the social stimulus, whereas LMK235-treated 16p11.2<sup>dp/+</sup> mice did not differ from WT in the amount of time spent interacting with the social stimulus (Fig. 4B,  $n = 7$ –12 mice/group,  $F_{\text{interaction}}(1,34) = 14.62, p = 0.0005$ , three-way ANOVA). No differences were observed between any group in the investigation time of the non-social stimulus (Fig. 4B). No change in body weight was observed in either 16p11.2<sup>dp/+</sup> or WT mice after LMK235 treatment (Fig. 4C,  $n = 7$ –17 mice,  $F_{\text{treatment}}(1,22) = 0.10, p = 0.76$ , two-way ANOVA). These data suggest that HDAC5 inhibition of 16p11.2<sup>dp/+</sup> mice can elicit improvement in social behavior.

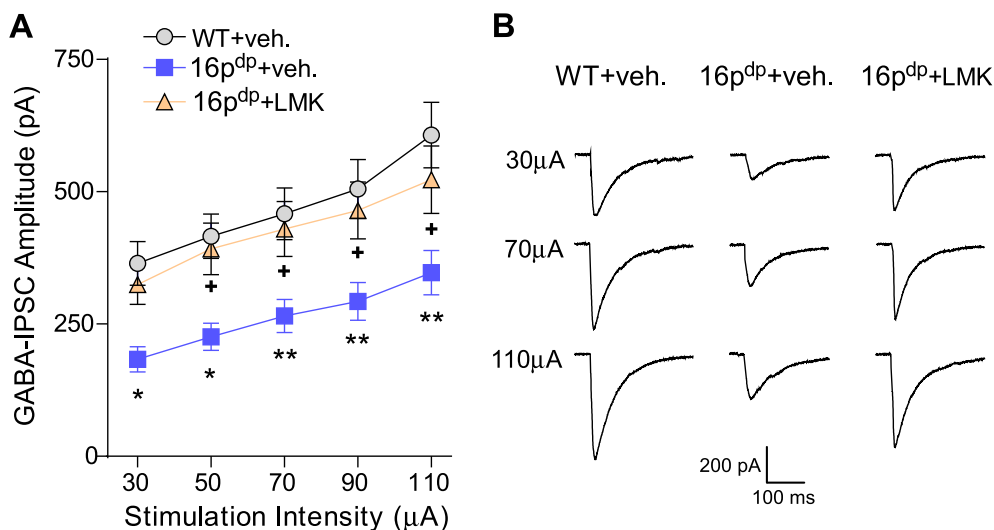


**Fig. 3.** Treatment with the HDAC5 inhibitor LMK235 restores GABAergic transmission in 16p11.2<sup>dp/+</sup> PFC pyramidal neurons. **A**, Summarized input-output curves of evoked GABA<sub>A</sub>R-mediated inhibitory postsynaptic currents (GABA<sub>A</sub>R-IPSC) in PFC pyramidal neurons from vehicle-treated WT mice, vehicle-treated 16p11.2<sup>dp/+</sup> mice, and LMK235-treated 16p11.2<sup>dp/+</sup> mice. +: 16p11.2<sup>dp/+</sup>+vehicle vs. 16p11.2<sup>dp/+</sup>+LMK235; \*: 16p11.2<sup>dp/+</sup>+vehicle vs. WT + vehicle. **B**, Representative GABA-IPSC traces. All data are presented as mean ± SEM. \**p* < 0.05, \*\**p* < 0.01, + *p* < 0.05.

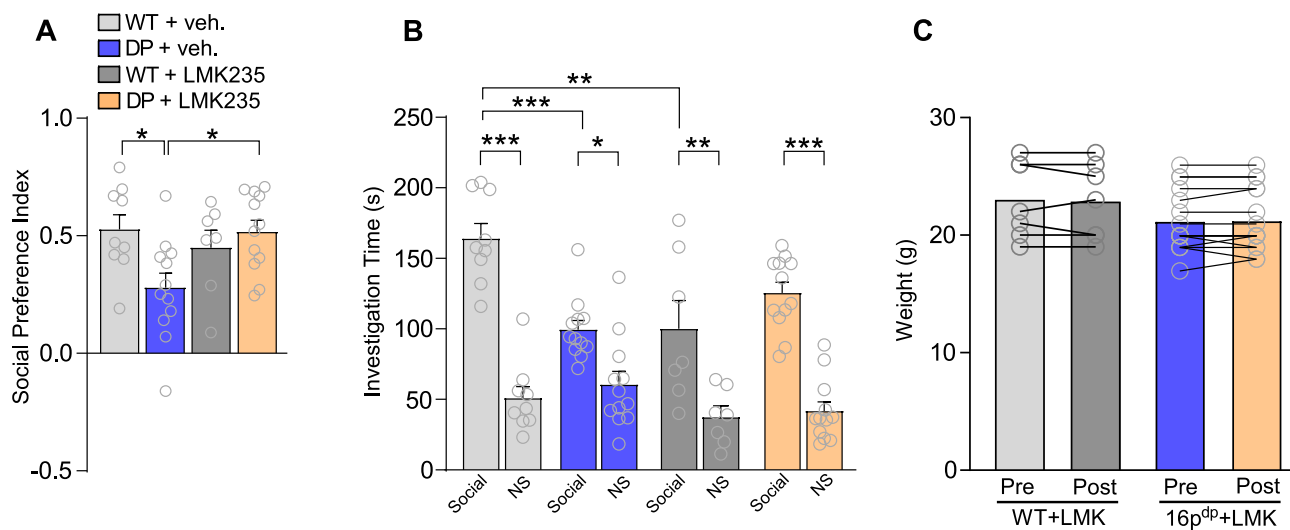


**Fig. 4.** HDAC5 inhibition ameliorates social deficits in 16p11.2<sup>dp/+</sup> mice. **A**, Bar graph comparing social preference indexes in the 3-chamber social preference test for vehicle-treated WT, vehicle-treated 16p11.2<sup>dp/+</sup> mice, LMK235-treated WT and LMK235-treated 16p11.2<sup>dp/+</sup> mice. **B**, Bar graphs comparing time spent interacting with a social stimulus (age-, sex- and strain-matched WT mouse) or a non-social stimulus (NS; wooden block) in the 3-chamber social preference test for the four groups. **C**, Bar graph comparing weights of WT and 16p11.2<sup>dp/+</sup> mice before and after 3-day treatment with LMK235. All data are presented as mean ± SEM. \**p* < 0.05, \*\**p* < 0.01, \*\*\**p* < 0.0001.

**4. Discussion**

In the current project, we report that HDAC5 is elevated in PFC of 16p11.2<sup>dp/+</sup> mice, which appears to be responsible for transcriptional repression of *Npas4* and concomitant GABAergic synaptic deficits. Moreover, systemic HDAC5 inhibition via LMK235 is sufficient to ameliorate the epigenetic aberration, GABAergic impairment, and social behavioral deficits in 16p11.2<sup>dp/+</sup> PFC. This suggests that pharmacological inhibition of HDAC5 may be a feasible therapeutic method for 16p11.2 duplication and related disorders.

We had previously identified *Npas4* downregulation as a core mechanistic driver of GABAergic dysfunction in 16p11.2<sup>dp/+</sup> PFC (Rein et al., 2021), though it was unclear what upstream molecular mechanisms were responsible for *Npas4* downregulation. Here we report that HDAC5 elevation results in reduced acetylation at the *Npas4* promoter in 16p11.2<sup>dp/+</sup> PFC, providing an upstream regulatory mechanism. Further investigations are required to identify the exact mechanism linking duplication of the genes in the 16p11.2 region with HDAC5 upregulation. Additionally, HDAC5 is an epigenetic enzyme which

exerts transcriptional control over a broad range of genes (Taniguchi et al., 2017). It is thus possible that HDAC5 dysregulation contributes to molecular and behavioral phenotypes in 16p11.2<sup>dp/+</sup> mice by driving aberrant expression of many genes in 16p11.2<sup>dp/+</sup> PFC. The extent of this HDAC5-mediated disruption in PFC and perhaps other brain areas in 16p11.2<sup>dp/+</sup> mice needs to be explored in future studies.

Here we demonstrate that systemic administration of the HDAC5-inhibitor LMK235 restores GABAergic transmission in 16p11.2<sup>dp/+</sup> PFC, which could be mediated by disinhibition of *Npas4* expression. However, other cellular mechanisms may also be involved, as HDAC5 regulates numerous genes in addition to *Npas4*. Furthermore, LMK235 also exerts inhibition of HDAC4 which may contribute to the behavioral and synaptic phenotypes observed in drug-treated 16p11.2<sup>dp/+</sup> mice. In our previous study, we found that restoring GABAergic transmission via *Npas4* was sufficient to elevate social behavior in 16p11.2<sup>dp/+</sup> mice (Rein et al., 2021). We thus postulate that the elevated GABA signaling in PFC of LMK235-treated 16p11.2<sup>dp/+</sup> mice underlies their observed improvements in the 3-chamber social preference task. However, it remains possible that these behavioral changes are influenced by other,

non-GABA-related mechanisms.

It is worth noting that LMK235-treated WT mice spent significantly less time interacting with the social stimulus in the 3-chamber social preference test than vehicle-treated WT animals, while the time spent interacting with the non-social cue was unchanged. These data suggest that systemic administration of LMK235 in healthy subjects may alter social behavior. However, the overall social preference index was unchanged in LMK235-treated WT mice, and systemic LMK235 administration treatment did not affect the weight of WT or 16p11.2<sup>dp/+</sup> mice. Regardless, the general safety of LMK235 and potential adverse effects of systemic HDAC5 inhibition should be further studied.

There are multiple lines of evidence implicating dysregulation of HDACs in epilepsy (Citiraro et al., 2017), and HDAC inhibitors such as valproic acid have a long history of being used to treat epilepsy (Eyal et al., 2004); however, the exact mechanisms regulating these therapeutic effects are poorly understood. Here we report that HDAC5 inhibition restores GABAergic synaptic transmission in 16p11.2<sup>dp/+</sup> PFC, providing a potential explanation for the anticonvulsant effects of HDAC inhibition. Interestingly, elevated expression of HDACs including HDAC5 has been reported in post-mortem hippocampal tissue of patients with mesial temporal lobe epilepsy (Srivastava et al., 2020). Thus, HDAC5-specific inhibition may offer therapeutic potential not only for 16p11.2 duplication, which is also associated with seizures (Rein and Yan, 2020), but also for unrelated cases of epilepsy. The translational potential for HDAC5 inhibition in 16p11.2 duplication syndrome awaits to be further investigated.

#### Author contributions

B.R. designed experiments, performed biochemical and electrophysiology experiments, analyzed data, and wrote the paper. M.C. performed some ChIP experiments, analyzed data, and wrote part of the paper. A.F. performed behavioral experiments. Q.C. performed biochemical experiments. Z.Y. designed experiments, supervised the project, and wrote the paper.

#### Declaration of interests

The authors report no competing financial or other interests.

#### Acknowledgements

We thank Xiaoqing Chen, Dr. Ping Zhong and Dr. Binglin Zhu for excellent technical support. This work was supported by Nancy Lurie Marks Family Foundation and National Institutes of Health (MH112237) to Z.Y. We also thank E.F. Trachtman and the Varanasi family for their kind donations.

#### References

- Bloodgood, B.L., Sharma, N., Browne, H.A., Trepman, A.Z., Greenberg, M.E., 2013. The activity-dependent transcription factor NPAS4 regulates domain-specific inhibition. *Nature* 503, 121–125.
- Cavallo, F., Troglio, F., Faga, G., Fancelli, D., Shyti, R., Trattaro, S., Zanella, M., D'Agostino, G., Hughes, J.M., Cera, M.R., Pasi, M., Gabriele, M., Lazzarin, M., Mihailovich, M., Kooy, F., Rosa, A., Mercurio, C., Varasi, M., Testa, G., 2020. High-

- throughput screening identifies histone deacetylase inhibitors that modulate GTF2I expression in 7q11.23 microduplication autism spectrum disorder patient-derived cortical neurons. *Mol. Autism* 11, 88.
- Citiraro, R., Leo, A., Santoro, M., D'Agostino, G., Constanti, A., Russo, E., 2017. Role of histone deacetylases (HDACs) in epilepsy and epileptogenesis. *Curr. Pharmaceut. Des.* 23, 5546–5562.
- Damborsky, J.C., Slaton, G.S., Winzer-Serhan, U.H., 2015. Expression of Npas4 mRNA in telencephalic areas of adult and postnatal mouse brain. *Front. Neuroanat.* 9, 145.
- Eyal, S., Yagen, B., Sobol, E., Altschuler, Y., Shmuel, M., Bialer, M., 2004. The activity of antiepileptic drugs as histone deacetylase inhibitors. *Epilepsia* 45, 737–744.
- Horev, G., Ellegood, J., Lerch, J.P., Son, Y.-E.E., Muthuswamy, L., Vogel, H., Krieger, A. M., Buja, A., Henkelman, R.M., Wigler, M., Mills, A.A., 2011. Dosage-dependent phenotypes in models of 16p11.2 lesions found in autism. *Proc. Natl. Acad. Sci. Unit. States Am.* 108, 17076–17081.
- Jenuwein, T., Allis, C.D., 2001. Translating the histone code. *Science* 293, 1074–1080.
- Lin, Y., Bloodgood, B.L., Hauser, J.L., Lapan, A.D., Koon, A.C., Kim, T.K., Hu, L.S., Malik, A.N., Greenberg, M.E., 2008. Activity-dependent regulation of inhibitory synapse development by Npas4. *Nature* 455, 1198–1204.
- Ma, K., Qin, L., Matas, E., Duffney, L.J., Liu, A., Yan, Z., 2018. Histone deacetylase inhibitor MS-275 restores social and synaptic function in a Shank 3-deficient mouse model of autism. *Neuropsychopharmacology* 43, 1779–1788.
- Pozhidayeva, D.Y., Farris, S.P., Goeke, C.M., Firsick, E.J., Townsley, K.G., Guizzetti, M., Ozburn, A.R., 2020. Chronic chemogenetic stimulation of the nucleus accumbens produces lasting reductions in binge drinking and ameliorates alcohol-related morphological and transcriptional changes. *Brain Sci.* 10.
- Qin, L., Ma, K., Wang, Z.J., Hu, Z., Matas, E., Wei, J., Yan, Z., 2018. Social deficits in Shank 3-deficient mouse models of autism are rescued by histone deacetylase (HDAC) inhibition. *Nat. Neurosci.* 21, 564–575.
- Rein, B., Ma, K., Yan, Z., 2020. A standardized social preference protocol for measuring social deficits in mouse models of autism. *Nat. Protoc.* 15, 3464–3477.
- Rein, B., Tan, T., Yang, F., Wang, W., Williams, J., Zhang, F., Mills, A., Yan, Z., 2021. Reversal of synaptic and behavioral deficits in a 16p11.2 duplication mouse model via restoration of the GABA synapse regulator Npas4. *Mol. Psychiatr.* 26, 1967–1979.
- Rein, B., Yan, Z., 2020. 16p11.2 copy number variations and neurodevelopmental disorders. *Trends Neurosci.* 43, 886–901.
- Srivastava, A., Banerjee, J., Dubey, V., Tripathi, M., Chandra, P.S., Sharma, M.C., Lalwani, S., Siraj, F., Doddamani, R., Dixit, A.B., 2020. Role of altered expression, activity and sub-cellular distribution of various histone deacetylases (HDACs) in mesial temporal lobe epilepsy with hippocampal sclerosis. *Cell Mol Neurobiol*, Epub ahead of print.
- Tan, T., Wang, W., Williams, J., Ma, K., Cao, Q., Yan, Z., 2019. Stress exposure in dopamine D4 receptor knockout mice induces schizophrenia-like behaviors via disruption of GABAergic transmission. *Schizophr. Bull.* 45, 1012–1023.
- Taniguchi, M., Carreira, M.B., Cooper, Y.A., Bobadilla, A.C., Heinsbroek, J.A., Koike, N., Larson, E.B., Balmuth, E.A., Hughes, B.W., Penrod, R.D., Kumar, J., Smith, L.N., Guzman, D., Takahashi, J.S., Kim, T.K., Kalivas, P.W., Self, D.W., Lin, Y., Cowan, C. W., 2017. HDAC5 and its target gene, Npas4, function in the nucleus accumbens to regulate cocaine-conditioned behaviors. *Neuron* 96, 130–144 e136.
- Trazzi, S., Fuchs, C., Viggiano, R., De Franceschi, M., Valli, E., Jedynek, P., Hansen, F.K., Perini, G., Rimondini, R., Kurz, T., Bartesaghi, R., Ciani, E., 2016. HDAC4: a key factor underlying brain developmental alterations in CDKL5 disorder. *Hum. Mol. Genet.* 25, 3887–3907.
- Wang, W., Rein, B., Zhang, F., Tan, T., Zhong, P., Qin, L., Yan, Z., 2018. Chemogenetic activation of prefrontal cortex rescues synaptic and behavioral deficits in a mouse model of 16p11.2 deletion syndrome. *J. Neurosci.* 38, 5939–5948.
- Wang, Z.J., Rein, B., Zhong, P., Williams, J., Cao, Q., Yang, F., Zhang, F., Ma, K., Yan, Z., 2021. Autism risk gene KMT5B deficiency in prefrontal cortex induces synaptic dysfunction and social deficits via alterations of DNA repair and gene transcription. *Neuropsychopharmacology* 46, 1617–1626.
- Wang, Z.J., Zhong, P., Ma, K., Seo, J.S., Yang, F., Hu, Z., Zhang, F., Lin, L., Wang, J., Liu, T., Matas, E., Greengard, P., Yan, Z., 2020. Amelioration of autism-like social deficits by targeting histone methyltransferases EHMT1/2 in Shank 3-deficient mice. *Mol. Psychiatr.* 25, 2517–2533.
- Yan, Z., Rein, B., 2021. Mechanisms of synaptic transmission dysregulation in the prefrontal cortex: pathophysiological implications. *Mol Psychiatry*, Epub ahead of print.
- Yuen, E.Y., Wei, J., Liu, W., Zhong, P., Li, X., Yan, Z., 2012. Repeated stress causes cognitive impairment by suppressing glutamate receptor expression and function in prefrontal cortex. *Neuron* 73, 962–977.